



OPEN ACCESS

EDITED BY

Jianfang Chen,
Ministry of Natural Resources, China

REVIEWED BY

Wei-Jen Huang,
National Sun Yat-sen University, Taiwan
Hui Gao,
Guangdong Ocean University, China

*CORRESPONDENCE

Yingxu Wu

✉ yingxu.wu@jmu.edu.cn

Di Qi

✉ qidi@jmu.edu.cn

RECEIVED 04 October 2023

ACCEPTED 09 January 2024

PUBLISHED 07 February 2024

CITATION

Yang W, Zhao Y, Wu Y, Chen Z, Gao X, Lin H,
Ouyang Z, Cai W, Chen L and Qi D (2024)
The impact of sea ice melt on the evolution
of surface $p\text{CO}_2$ in a polar ocean basin.
Front. Mar. Sci. 11:1307295.
doi: 10.3389/fmars.2024.1307295

COPYRIGHT

© 2024 Yang, Zhao, Wu, Chen, Gao, Lin,
Ouyang, Cai, Chen and Qi. This is an open-
access article distributed under the terms of
the [Creative Commons Attribution License
\(CC BY\)](https://creativecommons.org/licenses/by/4.0/). The use, distribution or reproduction
in other forums is permitted, provided the
original author(s) and the copyright owner(s)
are credited and that the original publication
in this journal is cited, in accordance with
accepted academic practice. No use,
distribution or reproduction is permitted
which does not comply with these terms.

The impact of sea ice melt on the evolution of surface $p\text{CO}_2$ in a polar ocean basin

Wei Yang¹, Yu Zhao², Yingxu Wu^{1*}, Zijie Chen², Xiang Gao¹,
Hongmei Lin³, Zhangxian Ouyang⁴, Weijun Cai⁴,
Liqi Chen¹ and Di Qi^{1*}

¹Polar and Marine Research Institute, College of Harbor and Coastal Engineering, Jimei University, Xiamen, China, ²Marine Science College, Nanjing University of Information Science & Technology, Nanjing, China, ³Key Laboratory of Global Change and Marine-Atmospheric Chemistry of Ministry of Natural Resources (MNR), Third Institute of Oceanography, Xiamen, China, ⁴School of Marine Science and Policy, University of Delaware, Newark, DE, United States

The strong CO_2 sink in Arctic Ocean plays a significant role in the global carbon budget. As a high-latitude oceanic ecosystem, the features of sea surface $p\text{CO}_2$ and air-sea CO_2 flux are significantly influenced by sea ice melt; however, our understanding of $p\text{CO}_2$ evolution during sea ice melt remains limited. In this study, we investigate the dynamics of $p\text{CO}_2$ during the progression of sea ice melt in the western Arctic Ocean based on data from two cruises conducted in 2010 and 2012. Our findings reveal substantial spatiotemporal variability in surface $p\text{CO}_2$ on the Chukchi Sea shelf and Canada Basin, with a boundary along the shelf breaks at depths of 250–500 m isobaths. On the Chukchi Sea shelf, strong biological consumption dominates $p\text{CO}_2$ variability. Moreover, in Canada Basin, the $p\text{CO}_2$ dynamics are modulated by various processes. During the active sea ice melt stage before sea ice concentration decreases to 15%, biological production through photosynthetic processes and dilution of ice melt water lead to a reduction in DIC concentration and subsequent decline in $p\text{CO}_2$. Further, these effects are counteracted by the air-sea CO_2 exchange at the sea surface which tends to increase seawater DIC and subsequently elevate surface $p\text{CO}_2$. Compared to the $p\text{CO}_2$ reduction resulting from biological production and dilution effects, the contribution of air-sea CO_2 exchange is significantly lower. The combined effects of these factors have a significant impact on reducing $p\text{CO}_2$ during this stage. Conversely, during the post sea ice melt stage, an increase in $p\text{CO}_2$ resulting from high temperatures and air-sea CO_2 exchange outweighs its decrease caused by biological production. Their combined effects result in a prevailing increase in sea surface $p\text{CO}_2$. We argue that enhanced air-sea CO_2 uptake under high wind speeds also contributes to the high sea surface $p\text{CO}_2$ observed in 2012, during both active sea ice melt stage and post sea ice melt stage. The present study reports, for the first time, the carbonate dynamics and $p\text{CO}_2$ controlling processes during the active sea ice melt stage. These findings have implications for accurate estimation of air-sea CO_2 fluxes and improved modeling simulations within the Arctic Ocean.

KEYWORDS

Western Arctic Ocean, $p\text{CO}_2$ dynamics, sea ice melt, sea ice concentration, wind speed

Highlights

- The decrease in DIC resulting from biological production and dilution of ice melt water tends to reduce $p\text{CO}_2$ during the active sea ice melt stage in Canada Basin, although it is counteracted by CO_2 uptake at the air-sea interface.
- The increase in $p\text{CO}_2$ resulting from high temperatures and air-sea CO_2 exchange outweighs its decrease caused by biological production, leading to elevated sea surface $p\text{CO}_2$ during the post sea ice melt stage in Canada Basin.
- The enhanced air-sea CO_2 uptake under high wind speeds also contributes to the high sea surface $p\text{CO}_2$ observed in 2012, during both active sea ice melt stage and post sea ice melt stage.

1 Introduction

Since the beginning of the first industrial revolution, anthropogenic activities have resulted in substantial carbon emissions into the atmosphere. Consequently, atmospheric carbon dioxide (CO_2) levels have continuously risen from 280 ppm in 1850 to 417 ppm in 2022. However, this increase accounts for only 49% of total carbon emissions, and 29% of emitted CO_2 has been absorbed by surface ocean (Friedlingstein et al., 2022). Due to the high solubility of CO_2 in low-temperature waters, the Arctic Ocean and its adjacent marginal seas serve as a significant CO_2 sink (Anderson and Kaltin, 2016; Yasunaka et al., 2018). Observations and model simulations have indicated that the Arctic Ocean absorbs 58–180 Tg C per year, accounting for 2%–7% of the global oceanic carbon sink (Manizza et al., 2013; Yasunaka et al., 2016; Mortenson et al., 2020). In recent decades, rapid and diverse changes, for example the increased seawater temperature, ice sheet melt, and an extended ice-free period, have occurred in Arctic ecosystems (Screen and Simmonds, 2010; Shepherd et al., 2012; Jeong et al., 2018). These changes exert a significant influence on sea surface $p\text{CO}_2$ and air-sea CO_2 fluxes. For instance, in the context of global warming, the Chukchi Sea has transitioned from being perennially covered by ice to becoming seasonally ice-free during the past two decades, and the summer CO_2 uptake has significantly increased by 1.4 ± 0.6 Tg C per decade (Ouyang et al., 2022).

Different from observations made in low/middle latitudinal marginal seas and open oceans, the features of sea surface $p\text{CO}_2$ and air-sea CO_2 flux in Arctic Ocean are significantly influenced by the presence of sea ice (Bates et al., 2011; Qi et al., 2020). During cold seasons, despite the elevated $p\text{CO}_2$ values beneath the sea ice, the air-sea CO_2 exchange is impeded by ice, resulting in relatively low CO_2 fluxes (Schuster et al., 2013; Cross et al., 2014; DeGrandpre et al., 2020). In contrast to observations in cold seasons, the water column stratification ensues during warm seasons when sea ice melts and freshwater input occurs. This

leads to a decrease in $p\text{CO}_2$ values and consequently enhances the CO_2 sink at the sea surface (Riedel et al., 2008). Moreover, the mixing of ice melt water featured low $p\text{CO}_2$ values, CaCO_3 dissolution, and photosynthesis during algal blooms would further decrease $p\text{CO}_2$ values and facilitate CO_2 dissolving into seawater (Fransson et al., 2009; Geilfus et al., 2012). However, this $p\text{CO}_2$ drawdown would be counteracted by the increased sea surface temperature and the strong CO_2 sink at the sea surface (Burgers et al., 2017; Islam et al., 2017; Pipko et al., 2017). In the seawater carbonate system, a frequent occurrence of high $p\text{CO}_2$ is observed in accordance with elevated SST values due to its decreased solubility at high temperatures (Wanninkhof et al., 2022). Additionally, the air-sea CO_2 exchange at the sea surface tends to increase seawater DIC in the Arctic Ocean, subsequently elevating seawater $p\text{CO}_2$ (Yang et al., 2023). Moreover, changes in wind fields, such as high wind speeds (>10 m/s) and upwelling-favorable wind, tend to upward transport the nutrient enriched water to subsurface. This nutrient supply significantly increases the net primary production (NPP), which consumes DIC and decreases the sea surface $p\text{CO}_2$ (Xu et al., 2023).

As previously mentioned, the spatiotemporal variability of hydrographic features and carbonate parameters during sea ice melt is influenced by various processes; however, their contributions to the dynamics of sea surface $p\text{CO}_2$ remain unclear. Previous studies have reported the $p\text{CO}_2$ dynamics during sea ice melt through model simulations and field measurements (e.g., Nomura et al., 2010; Fransson et al., 2017; DeGrandpre et al., 2020), but limited attention has been devoted to its changes prior to the melting process (DeGrandpre et al., 2020).

The Arctic Ocean serves as a conduit for water exchange between the Pacific and Atlantic oceans, and its biogeochemical cycling is influenced by lateral inputs of nutrients from sources like nutrient-rich inflows through the Barents Sea (North Atlantic) and Chukchi Sea (North Pacific) (Schuster et al., 2013). Characterized by intricate interactions and feedbacks among sea ice, ocean, and atmosphere, the Arctic Ocean plays a crucial role in the global climate system (Bates et al., 2011). In the context of global warming, there has been a significant decline in seasonal sea ice extent in the Arctic Ocean over the past four decades, accompanied by a more recent year-round decrease in sea ice extent, area, and volume (Polyakov et al., 2020). For instance, arctic sea ice extent has decreased at a rate of 13.1% per decade in September and 2.6% per decade in March; furthermore, the annual mean thickness of sea ice in the central Arctic Ocean reduced from 3.59 m to 1.25 m between 1975 and 2012 (Lindsay and Schweiger, 2015; Garcia-Soto et al., 2021). The reduction of sea ice content would hinder dense water formation while slowing down deep water circulation processes, leading to diminished CO_2 sequestration capacity (Semiletov et al., 2004).

In this study, we investigated the $p\text{CO}_2$ dynamics during two cruises in the western Arctic Ocean using underway measurements downloaded from an online database. Firstly, we identified the dominant processes governing the variations in $p\text{CO}_2$ and subsequently used a 1-D dynamic model to simulate $p\text{CO}_2$ values

in the western Arctic Ocean during sea ice melt. Finally, we quantified changes in $p\text{CO}_2$ between different stages of sea ice melt and elucidated their underlying controlling mechanisms.

2 Data and methods

2.1 Study area

The Arctic Ocean is a distinct basin surrounded by vast continental land masses. Based on hydrographic, topographic, and ocean circulation characteristics, the Arctic Ocean can be classified into various sub-regions such as the Norwegian Sea, Barents Sea, East Siberian Sea, Chukchi Sea, Beaufort Sea and the Canada Basin (Yasunaka et al., 2018). In this study, we divided the western Arctic Ocean into three sub-regions, as (1) the nutrient-rich Chukchi Sea shelf with a latitude range of 65–75°N; (2) the oligotrophic Canada Basin separated from the Chukchi Shelf along the shelf breaks at depths of 250–500 m isobaths; and (3) the Beaufort Sea separated from both the Chukchi Sea and Canada Basin by boundaries defined as longitude 152°W and latitude 72°N (Figure 1). Considering the different sea ice concentration (SIC) values presented in Table 1, we further divided the Canada Basin into two sub-regions, i.e. a sea ice covered zone (>77°N) and a rapid sea ice melt zone (<77°N). In Canada Basin, the water column can be categorized into five primary water masses, namely Pacific Winter Water (PWW), Alaska Coastal Water (ACW), Chukchi Summer Water (CSW), Early-Season Melt Water (ESMW), and Late-Season Melt Water (LSMW). During the warm seasons, ESMW and LSMW exert significant influence on the characteristics of surface water, confirming the impact of sea ice melt water (Qi et al., 2022a).

2.2 Data source

In this study, the *in situ* temperature, salinity, dissolved inorganic carbon (DIC), total alkalinity (TA), air and seawater $p\text{CO}_2$ values in the western Arctic Ocean were obtained from the Climate Variability and Predictability Experiment (CLIVAR) database (<https://www.ncei.noaa.gov/access/ocean-carbon-acidification-data-system/oceans/RepeatSections/>) (Figure 1). The data were collected during the 4th and 5th Chinese National Arctic Research Expedition (CHINARE) in 2010 and 2012, respectively. Detailed sampling and analysis methods for these two cruises can be found in Ouyang et al. (2020). Wind speed was obtained from JRA-55 reanalysis dataset (<http://search.diasjp.net/en/dataset/JRA55>), which has a spatial resolution of 0.5625° latitude/longitude and a temporal resolution of 3 hours (Japan Meteorological Agency/Japan, 2013). Near-surface winds were utilized to calculate the high wind frequency (HWF), representing the percentage of time when wind speed exceeds 10 m/s (Xu et al., 2023).

2.3 Air-sea CO_2 flux estimation

The net air-sea CO_2 flux (FCO_2 , $\text{mmol C m}^{-2} \text{d}^{-1}$) is calculated as (see Equation 1):

$$\text{FCO}_2 = k \times a \times (p\text{CO}_{2s} - p\text{CO}_{2a}) \times (1 - \text{SIC}) \quad (1)$$

where k represents the gas transfer velocity (m d^{-1}), a denotes the solubility of CO_2 ($\text{mol kg}^{-1} \text{atm}^{-1}$; Weiss, 1974); $p\text{CO}_{2s}$ and $p\text{CO}_{2a}$ represent the partial pressure of CO_2 in seawater and atmosphere, respectively, and their difference (defined as $\Delta p\text{CO}_2$) determines the direction of CO_2 transfer; SIC is the sea ice concentration with values ranging from 0 to 1. Please note that

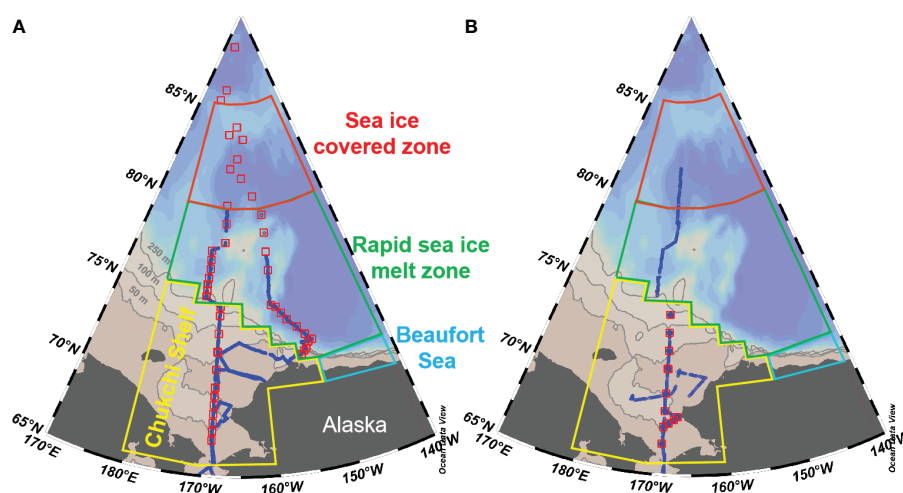


FIGURE 1

Maps showing the location of sampling stations (red squares) and underway measurements (blue dots) in the western Arctic Ocean during 2010 (A) and 2012 (B). Also shown are the boundary of different sub-regions following Ouyang et al. (2022): (1) Chukchi Sea shelf with latitude of 65–75°N, as shown by the yellow line; (2) Canada Basin, separated from the Chukchi Shelf along the 250–500 m isobaths; (3) the Beaufort Sea, separated from the Chukchi Sea and Canada Basin along 152°W and 72°N, respectively. Considering the different sea ice concentrations during warm seasons, we further divided the Canada Basin into two sub-regions with a latitude of 80°N, i.e. the sea ice covered zone and the rapid sea ice melt zone (Ouyang et al., 2022).

TABLE 1 Summary of sea ice concentration (SIC), high wind frequency (HWF) and wind speed in different sub-regions.

Sub-regions	Date	Voyage	SIC	HWF	Wind Speed (m s ⁻¹)
Chukchi Sea	20100720	Forward	0.063	0.081	5.81
	20100829	Return	0.018	0	5.09
	20120718	Forward	0.130	0.019	5.83
	20120907	Return	0.019	0.168	7.44
Sea ice covered zone in Canada Basin	20100730-20100826	Forward and return	0.694	0	3.30
	20120904	Forward and return	0.288	0.042	6.47
Sea ice melt zone in Canada Basin	20100724	Forward	0.524	0.114	5.11
	20100826	Return	0.092	0.021	4.89
	20120906	Return	0	0.194	7.23

Note HWF is high wind frequency (wind speed >10 m s⁻¹).

Please note that these average values were obtained from model simulation following methods described in Xu et al. (2023).

the SIC data utilized in this study were obtained from the NSIDC (Nation Snow and Ice Data Center) database (<https://nsidc.org/data/nsidc-0079/versions/3>).

The gas transfer velocity was calculated following Wanninkhof (2014), as (see Equation 2):

$$k = 0.251 \times U_{10}^2 \times (Sc/660)^{-0.5} \quad (2)$$

where U_{10} represents wind speed at 10 m height. Sc corresponds to Schmidt number for CO₂, which was determined using equations in Wanninkhof (2014).

2.4 Modeling the pCO₂ values with a 1-D dynamic approach

In this study, a mass balance model was used to simulate the pCO₂ dynamics during sea ice melt. For each simulation step (Δt , 1 day in this study), sea surface pCO₂ was calculated from TA and DIC at the corresponding step. A change in DIC inventory for a time step, Δt , in the surface mixed layer (defined as ΔDIC_t) is calculated as follows (see Equation 3):

$$\Delta DIC_t = (FCO_{2t} + NCP_t) \times \Delta t / (MLD \times \rho) + \Delta DIC_{(diluted)t} \quad (3)$$

where FCO_{2t} , NCP_t , and $\Delta DIC_{(diluted)t}$ indicate the changes in DIC inventory ($\mu\text{mol kg}^{-1}$) induced by air-sea CO₂ flux ($\text{mmol C m}^{-2} \text{d}^{-1}$), net community production (NCP , $\text{mmol C m}^{-2} \text{d}^{-1}$), and melt water dilution ($\Delta DIC_{(diluted)t}$, $\mu\text{mol kg}^{-1}$) at simulation time step t , respectively. MLD (m) and ρ (set as $1.021 \times 10^3 \text{ kg m}^{-3}$) are the mixed layer depth and density of surface seawater.

During the model simulation, we assumed that the dilution of ice melt water will change the concentrations of DIC and TA in the seawater at a same rate, which has been previously proposed and utilized by Qi et al. (2022b). In Arctic Ocean, the TA and DIC values in surface water were set as 1959 $\mu\text{mol kg}^{-1}$ and 1880 $\mu\text{mol kg}^{-1}$, respectively, which were much higher than that in the ice melt water end-member (TA=400 $\mu\text{mol kg}^{-1}$, DIC=450 $\mu\text{mol kg}^{-1}$) (Yang et al., 2023). The mixing of ice melt water have negligible influence on the

TA/DIC ratio in surface water, which is close to 1:1. Therefore, any changes in DIC induced by dilution (defined as $\Delta DIC_{(diluted)t}$) can be quantified as follows (see Equation 4):

$$\Delta DIC_{(diluted)t} = (TA_{t+1} - TA_t) / TA_t \times DIC_t \quad (4)$$

where $(TA_{t+1} - TA_t) / TA_t$ is the changing rate in TA during sea ice melt. And DIC at time step $t+1$ is iteratively calculated as follows (see Equation 5):

$$DIC_{t+1} = DIC_t + \Delta DIC_t \quad (5)$$

Due to the dilution caused by ice melt water, TA in the seawater decreased continuously from its initial values at a SIC of 95% to low values at a SIC of 0% during the sea ice melt. Subsequently, TA remained constant during the ice free period. With the new DIC and TA for the next simulation step, a new pCO₂ is calculated, and this simulation process repeats until the last day.

3 Results

3.1 Distributions of sea surface temperature, salinity and pCO₂ in the western Arctic Ocean

The surface distributions of temperature (SST), salinity (SSS), and pCO₂ during both cruises are shown in Figure 2, which exhibited significant spatial variability. In 2010, SST ranged from -2.0 to 8.0 °C, exhibiting a latitudinal decreasing trend (Figure 2A). The Chukchi Sea exhibited the highest SST values, followed by the rapid sea ice melt zone and the sea ice covered zone in Canada Basin. This distribution pattern aligns with previous studies conducted by Sun et al. (2017) and Yang et al. (2023), which can be attributed to reduced solar radiation at higher latitudes and the influence of warm Pacific surface water on the Chukchi Sea shelf (Zheng et al., 2021). SSS displayed their highest values on the Chukchi Sea shelf, ranging from 29 to 32.5, while relatively lower values were observed in Canada Basin, ranging from 25.5 to 29 (Figure 2B). As mentioned

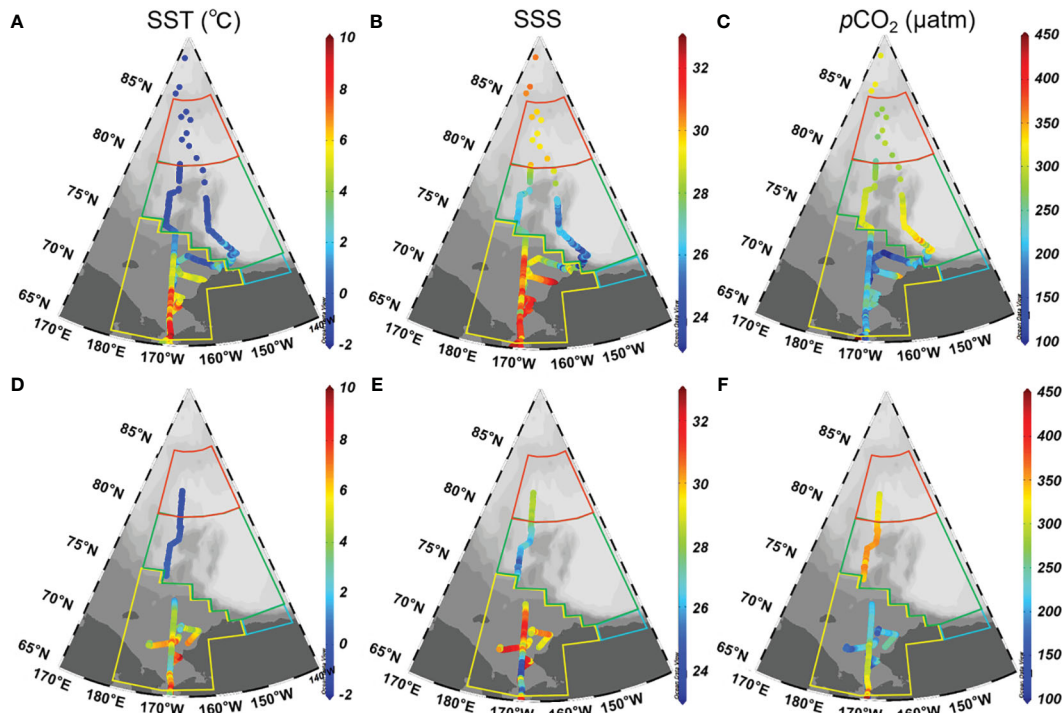


FIGURE 2

Surface distributions of temperature (left panels), salinity (middle panels), and $p\text{CO}_2$ (right panels) in the western Arctic Ocean in 2010 (A–C) and 2012 (D–F). In (A, B), SST and SSS observed north of 80°N are sourced from bottle data. In (C), $p\text{CO}_2$ were calculated from DIC and TA using the CO2SYS program (Pierrot et al., 2006), which employed dissociation constants for carbonic acid from Mehrbach et al. (1973), as refitted by Dickson and Millero (1987), along with the dissociation constant for HSO_4^- determined by Dickson (1990). The relationship between total boron and salinity followed Upstrom (1967).

earlier, high salinity on the Chukchi Sea shelf reflects the influence of Pacific Source Water, whereas low salinity surface water in Canada Basin is likely diluted by ice melt water (Geilfus et al., 2012). The sea surface $p\text{CO}_2$ during this cruise exhibited a range of 100–350 μatm (Figure 2C). Low $p\text{CO}_2$ values were observed on the Chukchi Sea shelf, whereas high values were observed in Canada Basin. On the Chukchi Sea shelf, the low $p\text{CO}_2$ values can be attributed to the high biological production sustained by nutrient-rich Bering Strait through flow (Tu et al., 2021; Zheng et al., 2021). In Canada Basin, sea ice exerts a significant influence on regulating the dynamics of sea surface $p\text{CO}_2$ during both sea ice formation and melt processes. The evolution of sea surface $p\text{CO}_2$ during the sea ice melt will be further quantified in the subsequent discussion.

In 2012, SST, SSS, and $p\text{CO}_2$ ranged -1 – 7.5°C , 25.0–32.0, and 180–360 μatm , respectively (Figures 2D–F). Due to the influence of Pacific Water, the Chukchi Sea shelf exhibited significantly higher SST and SSS compared to the Canada Basin, which is consistent with the observations made in 2010. In contrast to the observations in Canada Basin, the sea surface $p\text{CO}_2$ on the Chukchi Sea shelf was observed to be at its lowest level.

3.2 Distributions of SIC, HWF and wind speed in the western Arctic Ocean

As shown in Table 1, the surface water in the northernmost sea ice covered zone was predominantly encompassed by sea ice with

SIC values ranging from 0.29 to 0.69 throughout the sampling period. In the rapid sea ice melt zone, distinct SIC values were recorded during these three voyages, ranging from 0 to 0.524. On the Chukchi Sea shelf, there was a minor influence of sea ice melt as evidenced by low SIC values ranging from 0.02 to 0.13. The highest HWF and wind speed were observed during the cruise in 2012.

4 Discussion

4.1 Controlling processes to the dynamics of sea surface $p\text{CO}_2$ in Canada Basin

4.1.1 Temperature effect

During both cruises, the variability of SST ranged from -1.6°C to 4.0°C , which could significantly impact the distribution patterns of surface $p\text{CO}_2$. To assess the influence of temperature on $p\text{CO}_2$ variability, we plotted the relationship between $\ln p\text{CO}_2$ and SST (Figure 3A). In 2010, a positive correlation was observed with an equation of $\ln p\text{CO}_2 = 0.0394 \times \text{SST} + 5.7704$ ($R^2 = 0.38$, $p < 0.05$). Wanninkhof et al. (2022) suggested an exponential increase in $p\text{CO}_2$ with rising temperature at a rate of $4.13\% \text{ }^\circ\text{C}^{-1}$. Although the observed slope was nearly consistent with the theoretical value of 0.0413, the correlation coefficient is only 0.6 ($R = 0.6$). This result indicates that although temperature is a significant controlling factor, it cannot fully explain the variability in $p\text{CO}_2$ within the

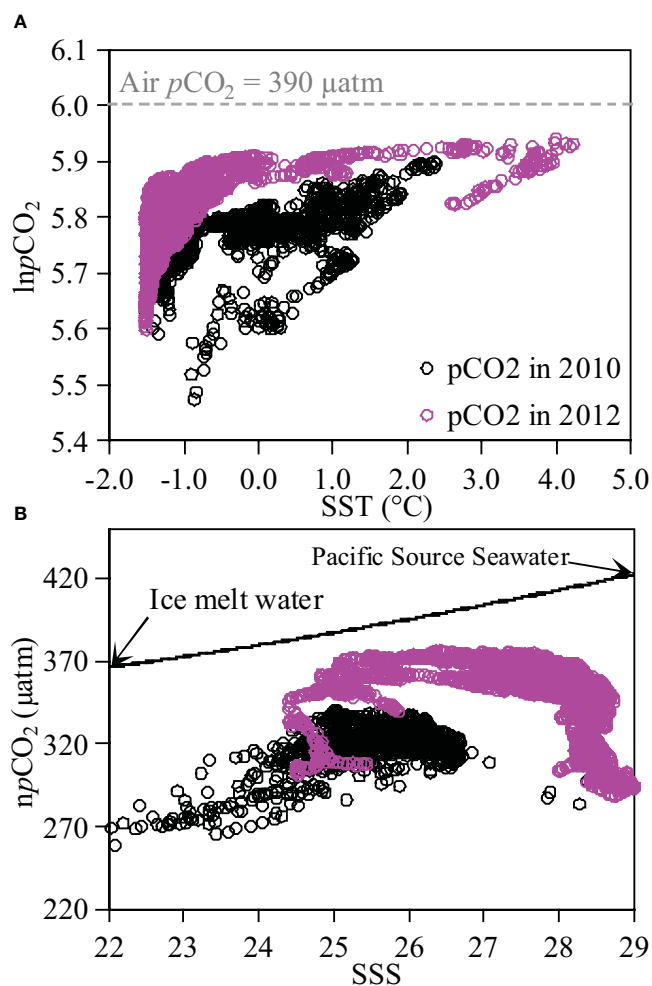


FIGURE 3

Relationships of $\ln p\text{CO}_2$ vs. sea surface temperature, SST ($\ln p\text{CO}_2$ -SST, (A) and $\ln p\text{CO}_2$ vs. sea surface salinity, SSS ($\ln p\text{CO}_2$ -SSS, panel b) for surface water in Canada Basin in 2010 and 2012. In panel a, dashed line indicate the logarithm of air $p\text{CO}_2$. In (B), black arrows represent the end-members of ice melt water and Pacific Source Seawater with end-member values sourced from Qi et al. (2020) and Yang et al. (2023); solid line represent the hypothetical conservative mixing line between these two end-members.

Canada Basin. In 2012, there was also a positive correlation relationship between $\ln p\text{CO}_2$ and SST for surface water with an equation of $\ln p\text{CO}_2 = 0.0702x + 5.8696$ ($R^2 = 0.26$, not shown in the figure), but this relationship alone cannot fully explain variation in $p\text{CO}_2$.

4.1.2 Dilution of ice melt water

In Canada Basin, it has been suggested that the offshore surface water is influenced by the dilution of ice melt water and Pacific Source Seawater (Qi et al., 2020). Using end-member values of $S = 33.215 \pm 0.012$, $\text{TA} = 2242.2 \pm 6.9 \mu\text{mol kg}^{-1}$, $\text{DIC} = 2159.1 \pm 0.3 \mu\text{mol kg}^{-1}$ for Pacific Source Seawater and $S = 0$, $\text{TA} = 400 \mu\text{mol kg}^{-1}$, $\text{DIC} = 450 \mu\text{mol kg}^{-1}$ for ice melt water (Yang et al., 2023), we calculated the proportions of ice melt water at different salinities. During both cruises, the fractions of ice melt water ranged from 12.7% to 27.7%. We further calculated the conservative $p\text{CO}_2$ values at different salinities, and the result suggested a $p\text{CO}_2$ value of 368 μatm at salinity of 22, and a $p\text{CO}_2$ value of 411 μatm at salinity of 29. The observed difference in $p\text{CO}_2$ (43 μatm) can be attributed to

the dilution effect. We also examined the relationship between $\ln p\text{CO}_2$ and SSS to investigate the influence of water mass mixing on the variability of sea surface $p\text{CO}_2$ in Canada Basin (Figure 3B). In this study, $\ln p\text{CO}_2$ was normalized to 0 $^{\circ}\text{C}$ following the method of Wanninkhof et al. (2022). Consequently, no significant correlation was observed between $\ln p\text{CO}_2$ and SSS, indicating that other processes may exert a stronger impact on the spatial variability of sea surface $p\text{CO}_2$ than mixing during both cruises.

4.1.3 Air-sea CO_2 flux

In Canada Basin, there was an average difference of -25 to -80 μatm between $p\text{CO}_2$ values in surface water and the overlying atmosphere (Table 2), indicating a net uptake of CO_2 during both cruises. Using average SIC values and wind speeds summarized in Table 1, we estimated the air-sea CO_2 flux during the sampling period, and the results are summarized in Table 2. Consequently, the instantaneous air-sea CO_2 fluxes varied from -1.6 to -4.3 $\text{mmol C m}^{-2} \text{d}^{-1}$ (Table 2; negative values indicate a CO_2 sink). Our estimated CO_2 flux was almost consistent with Yasunaka et al. (2016) of $-4 \pm 4 \text{ mmol}$

TABLE 2 Summary of sea surface temperature (SST), sea surface salinity (SSS), sea surface $p\text{CO}_2$, air-sea $\Delta p\text{CO}_2$, CO_2 flux, and average mixed layer depth (m) in Canada Basin.

Date	Voyage	SST (°C)	SSS	$p\text{CO}_{2\text{in-situ}}$ (μatm)	Air-sea $\Delta p\text{CO}_2$ (μatm)	CO_2 flux ($\text{mmol C m}^{-2} \text{d}^{-1}$)	MLD (m)
20100724	Forward	0.3 ± 0.9	25.4 ± 1.8	306 ± 41	-71 ± 41	-1.6 ± 1.6	13.2
20100826	Return	-0.5 ± 1.2	26.8 ± 1.2	292 ± 35	-80 ± 34	-4.3 ± 1.8	16.2
20120906	Return	0.3 ± 0.1	25.8 ± 0.5	351 ± 19	-25 ± 19	-3.3 ± 2.4	18.8

Please note that the mixed layer depth (MLD) during both voyages was obtained using methods described in Xu et al. (2023).

$\text{C m}^{-2} \text{d}^{-1}$, Manizza et al. (2019) of $-2.5 \pm 0.2 \text{ mmol C m}^{-2} \text{d}^{-1}$, Bates and Mathis (2009) of $-1.7 \sim -4.2 \text{ mmol C m}^{-2} \text{d}^{-1}$, and Islam et al. (2017) of $-2.5 \pm 2.6 \text{ mmol C m}^{-2} \text{d}^{-1}$ in Arctic Ocean, but was lower than Ouyang et al. (2022) of $-5.0 \text{ mmol C m}^{-2} \text{d}^{-1}$ in Canada Basin, Sun et al. (2017) of $-8.6 \pm 1.4 \text{ mmol C m}^{-2} \text{d}^{-1}$ and Burgers et al. (2017) of $-12 \text{ mmol C m}^{-2} \text{d}^{-1}$ in Arctic Ocean.

Here we conducted a preliminary estimation of DIC and subsequently the $p\text{CO}_2$ increase during sea ice melt. Assuming an average CO_2 flux of $-3.0 \text{ mmol C m}^{-2} \text{d}^{-1}$ during these three voyages (Table 2), an ice melt period of 80 days during warm seasons (from $\text{DSR}=-40$ to $\text{DSR}=40$), and an average MLD of 16 m that obtained using methods described in Xu et al. (2023) (Table 2), it can be inferred that the air-sea CO_2 exchange at the sea surface would result in a rise in seawater DIC by $15 \mu\text{mol kg}^{-1}$. Based on the definition of Revelle factor (RF), $p\text{CO}_2$ variability caused by the air-sea CO_2 exchange can be calculated as: $\text{RF} \times p\text{CO}_{2\text{water}} \times \Delta\text{DIC}_f / \text{DIC}_{\text{water}}$ (Harry et al., 1979; Egleston et al., 2010). The results suggest that, during sea ice melt, air-sea CO_2 exchange at the sea surface would lead to an increase in seawater $p\text{CO}_2$ by $40 \mu\text{atm}$ in Canada Basin.

4.1.4 Sea ice concentration

In Canada Basin, a significant negative relationship is observed between SIC and sea surface $p\text{CO}_2$ ($p\text{CO}_2 = -46.14 \times \text{SIC} + 343.43$, $R^2 = 0.47$, Figure 4). The surface $p\text{CO}_2$ tends to decrease with increasing SIC, exhibiting lower values in areas where $\text{SIC} > 0.5$ and higher values in open water with an SIC of 0. In Arctic ecosystems, low SIC would facilitate CO_2 dissolution into seawater, leading to

increased seawater DIC and surface $p\text{CO}_2$. During both cruises, the observed sea surface $p\text{CO}_2$ was measured at $343 \mu\text{atm}$ when $\text{SIC}=0$, and decreased to $297 \mu\text{atm}$ when $\text{SIC}=1$. The calculated difference in $p\text{CO}_2$ amounts to $46 \mu\text{atm}$.

4.1.5 Biological consumption

In Arctic Ocean, the higher nutrient supply and subsequent biological consumption of DIC result in a significant net uptake of CO_2 . Previous studies have reported the NCP values in this region, ranging from 1.88 to $7 \text{ mmol C m}^{-2} \text{d}^{-1}$ (Cai et al., 2010; Islam et al., 2017; DeGrandpre et al., 2019; Ouyang et al., 2022). Using an NCP value of $1.88 \text{ mmol C m}^{-2} \text{d}^{-1}$ (Cai et al., 2010), and an ice melt period of 80 days, it can be inferred that biological consumption would lead to a decrease in seawater DIC by $9 \mu\text{mol kg}^{-1}$ and subsequently reduce seawater $p\text{CO}_2$ by $24 \mu\text{atm}$.

4.1.6 Wind speed

In the estimation of air-sea CO_2 flux, higher wind speeds lead to an increased gas transfer velocity, thereby resulting in a higher CO_2 flux (see Equation 2). In Arctic Ocean, the intensified CO_2 sink under high wind speeds would elevate seawater DIC concentrations and subsequently increase $p\text{CO}_2$. Here we utilized the HWF obtained from model simulations to characterize the intensity of wind speeds (for more details on the model simulation, please refer to Xu et al. (2023)), and their respective results were presented in Table 1. Consequently, HWF and wind speeds exhibited notable increases in 2012 than in 2010, which may also contribute to higher $p\text{CO}_2$ in 2012.

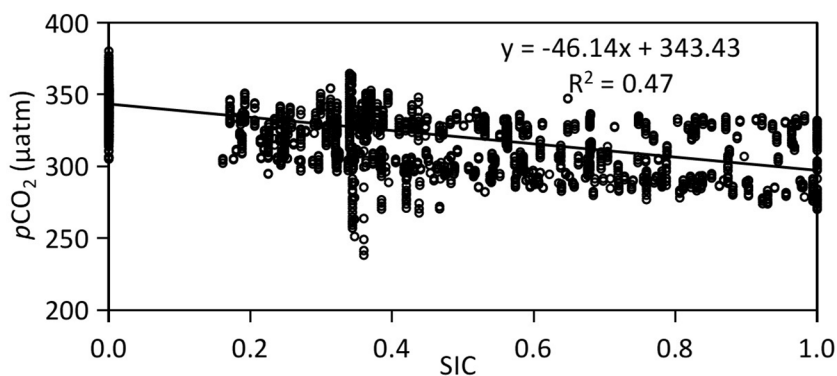


FIGURE 4

Linear relationship between surface $p\text{CO}_2$ and sea ice concentration (SIC) in Canada Basin with data collected during both 2010 and 2012.

4.2 Modeling the sea surface $p\text{CO}_2$ during sea ice melt

4.2.1 Results from a 1-D dynamic model

To assess changes in sea surface $p\text{CO}_2$ during sea ice melt, we utilized the definition of days since ice retreat (DSR) in our results description and model simulation. Firstly, the day of ice retreat (DOR) is defined as the day when SIC falls below 15%. Then, we calculate the temporal difference between DOR and the day of field observation (DOF), which represents DSR. A positive or negative DSR indicates that the corresponding DOR occurred earlier or later than DOF. The specific values of DSR and SIC during these two cruises can be found in the Supplementary Material provided by Qi et al. (2022b).

In the present study, we divided the sampling period during both cruises into three distinct stages, the pre-retreat stage ($\text{DSR} < -40$), an active sea ice melt stage ($-40 < \text{DSR} < 0$), and a post sea ice melt stage ($\text{DSR} > 0$). Consequently, DSR values for $p\text{CO}_2$ measurements in 2010 were predominantly negative ($\text{DSR} < 0$), representing an active sea ice melt stage. Conversely, DSR values in 2012 were positive ($\text{DSR} > 0$), representing a post sea ice melt stage. As shown in Figure 5, during the active sea ice melt stage in 2010, $p\text{CO}_2$ measurements displayed a scattered distribution pattern; however, they demonstrated an increasing trend during the post sea ice melt stage in 2012.

In order to gain a better understanding of variations in $p\text{CO}_2$ during sea ice melt, we extended our simulation time to the early melt period. Consequently, our modeled results covered the DSR from -50 days to the maximum DSR recorded during these two

cruises (50 days). The initial values and model settings were derived from Qi et al. (2022b). Briefly, the initial SST, SSS, $p\text{CO}_2$, and TA were averaged from observations beneath the sea ice for the period 2011-2020 when DSR was less than -40. Their respective values were set at -1.0°C , 27.1, 330 μatm , and 1959 $\mu\text{mol kg}^{-1}$. During the sea ice retreat period ($-50 < \text{DSR} < 0$), we assumed that SST linearly increased from its initial value to the mean SST over $-5 < \text{DSR} < 5$. Simultaneously, ice concentration linearly decreased from 95% to 0%, while SSS and TA decreased gradually from their initial values to their respective means over $-5 < \text{DSR} < 5$. The values of SST, SSS, and TA at $\text{DSR} = 0$ were set to -0.7°C , 26, and 1886 $\mu\text{mol kg}^{-1}$, respectively. During the ice free period ($\text{DSR} > 0$), SSS and TA remained constant while allowing SST to increase up to a maximum value of 1.4°C at $\text{DSR} = 60$. A NCP value of 1.88 $\text{mmol C m}^{-2} \text{d}^{-1}$ was assigned for the period between $-40 < \text{DSR} < 50$ to reflect weak primary production in the study area (Cai et al., 2010), whereas a value of 0 $\text{mmol C m}^{-2} \text{d}^{-1}$ was used for the period between $-50 < \text{DSR} < -40$. An averaged MLD of 16 m was consistently applied throughout the simulation (Table 2). Two average wind speeds, 4 m s^{-1} recorded during July and August in 2010, and 7 m s^{-1} observed during July, August, and September in 2012, were considered for CO_2 flux estimation and model simulation.

The evolution of seawater $p\text{CO}_2$ during sea ice melt in Canada Basin was simulated with a wind speed of 4.0 m s^{-1} , and their result was shown in Figure 5. During the pre-retreat stage, no significant change was observed in the simulated seawater $p\text{CO}_2$. Subsequently, a decreasing trend in $p\text{CO}_2$ was observed during the active sea ice melt stage. Following this stage, there was a continuous increase in the simulated seawater $p\text{CO}_2$ during the post sea ice melt stage.

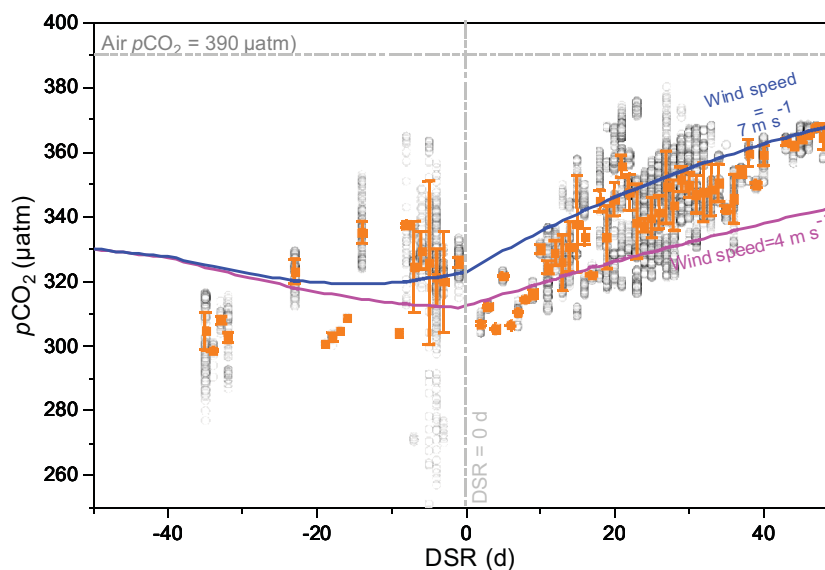


FIGURE 5

Relationships between $p\text{CO}_2$ and days since ice retreat (DSR) in Canada Basin during the cruise both in 2010 and 2012 (gray circles). Orange squares and error bars indicate the average values. During both cruises, DSR values for $p\text{CO}_2$ measurements in 2010 were predominantly negative ($\text{DSR} < 0$), representing an active sea ice melt stage. Conversely, DSR values in 2012 were positive ($\text{DSR} > 0$), representing a post sea ice melt stage. The horizontal dashed line is the atmospheric $p\text{CO}_2$ of 390 μatm , and the vertical dashed line is $\text{DSR} = 0$ d. Solid lines are the simulated seawater $p\text{CO}_2$ using a 1-D dynamic approach at a wind speed of 4 m s^{-1} (pink line) and 7 m s^{-1} (blue line), with initial values and model settings derived from Qi et al. (2022b).

When using a higher wind speed of 7.0 m s^{-1} , it was noted that $p\text{CO}_2$ exhibited a decreasing trend when $\text{DSR} < -10$ but an increasing trend when $\text{DSR} > -10$. In comparison to the $p\text{CO}_2$ values simulated at a wind speed of 4.0 m s^{-1} , the modeled $p\text{CO}_2$ with a wind speed of 7.0 m s^{-1} showed significantly higher values; exhibiting a difference of $11 \text{ } \mu\text{atm}$ at $\text{DSR}=0$ and reaching up to $25 \text{ } \mu\text{atm}$ at $\text{DSR}=50$.

4.2.2 Quantifying the controlling processes to the $p\text{CO}_2$ dynamics during sea ice melt

Here, we quantified the controlling processes to $p\text{CO}_2$ dynamics during sea ice melt at two stages, the active sea ice melt stage (from $\text{DSR}=-40$ to $\text{DSR}=0$) and the post sea ice melt stage (from $\text{DSR}=0$ to $\text{DSR}=50$), with modeled carbonate parameters at $\text{DSR}=-40, 0$, and 50 . To assess the impact of temperature effects on $p\text{CO}_2$ dynamics, we firstly calculated $p\text{CO}_2$ values at different SSTs while keeping DIC and TA constant for each stage. The difference in $p\text{CO}_2$ values represented changes attributed to temperature effects. For biological production and air-sea CO_2 exchange, we first calculated the variability in DIC resulting from the biological consumption (referred to as $\Delta\text{DIC}_{\text{Bio}}$) and air-sea CO_2 flux (referred to as $\Delta\text{DIC}_{\text{Flux}}$) as $\text{NCP}/(\text{MLD} \times \rho)$ and $\text{FCO}_2/(\text{MLD} \times \rho)$, respectively. Subsequently, these DIC consumption/addition values were subtracted/added to the observed DIC data (referred to as $\text{DIC}^{\text{obs-Bio}}$ and $\text{DIC}^{\text{obs-Flux}}$), allowing us to calculate seawater $p\text{CO}_2$ with the new DIC concentrations. The difference between these calculated and observed $p\text{CO}_2$ values indicates changes attributed to biological production and air-sea CO_2 exchange. Finally, the DIC changes resulted from the dilution of ice melt water was estimated as $\Delta\text{DIC} - \Delta\text{DIC}_{\text{Bio}} - \Delta\text{DIC}_{\text{Flux}}$ to balance the overall DIC budget. Its impact on $p\text{CO}_2$ variability could be determined using methods described above.

During the sea ice melt, the contributions of different processes to the dynamics of $p\text{CO}_2$ under a wind speed of 4 m s^{-1} were summarized in Figure 6A. During the active sea ice melt stage, the increase in SST of $0.24 \text{ } ^\circ\text{C}$ only resulted in a rise in $p\text{CO}_2$ by $4 \text{ } \mu\text{atm}$. Over a time scale of 40 days, biological production and air-sea CO_2 exchange led to a decrease and increase in DIC by $5 \text{ } \mu\text{mol kg}^{-1}$ and $5 \text{ } \mu\text{mol kg}^{-1}$, respectively, which would alter seawater $p\text{CO}_2$ by $-15 \text{ } \mu\text{atm}$ and $15 \text{ } \mu\text{atm}$ correspondingly. Furthermore, the dilution effect caused by ice melt water further reduced seawater $p\text{CO}_2$ by $16 \text{ } \mu\text{atm}$. Consequently, compared to its reduction resulting from biological production and dilution effects, the contribution of air-sea CO_2 exchange towards increasing $p\text{CO}_2$ was significantly lower. The combined effects of biological production, dilution effects, and air-sea CO_2 exchange have a significant impact on reducing $p\text{CO}_2$ during this stage. During the post sea ice melt stage, there was an observed increase in $p\text{CO}_2$ by $45 \text{ } \mu\text{atm}$. The increase in SST by $2.1 \text{ } ^\circ\text{C}$ would elevate $p\text{CO}_2$ by $32 \text{ } \mu\text{atm}$, while biological production and air-sea CO_2 exchange would lead to a decrease and increase respectively in seawater $p\text{CO}_2$ by $22 \text{ } \mu\text{atm}$ and $37 \text{ } \mu\text{atm}$ due to variability in DIC of $-7 \text{ } \mu\text{mol kg}^{-1}$ and $11 \text{ } \mu\text{mol kg}^{-1}$. The influence of ice melt water is negligible during the post sea ice melt stage. Consequently, the increase in $p\text{CO}_2$ resulting from high temperatures and air-sea CO_2 exchange outweighs its decrease caused by biological production. The combined effects of temperature effect, biological production, and air-sea CO_2

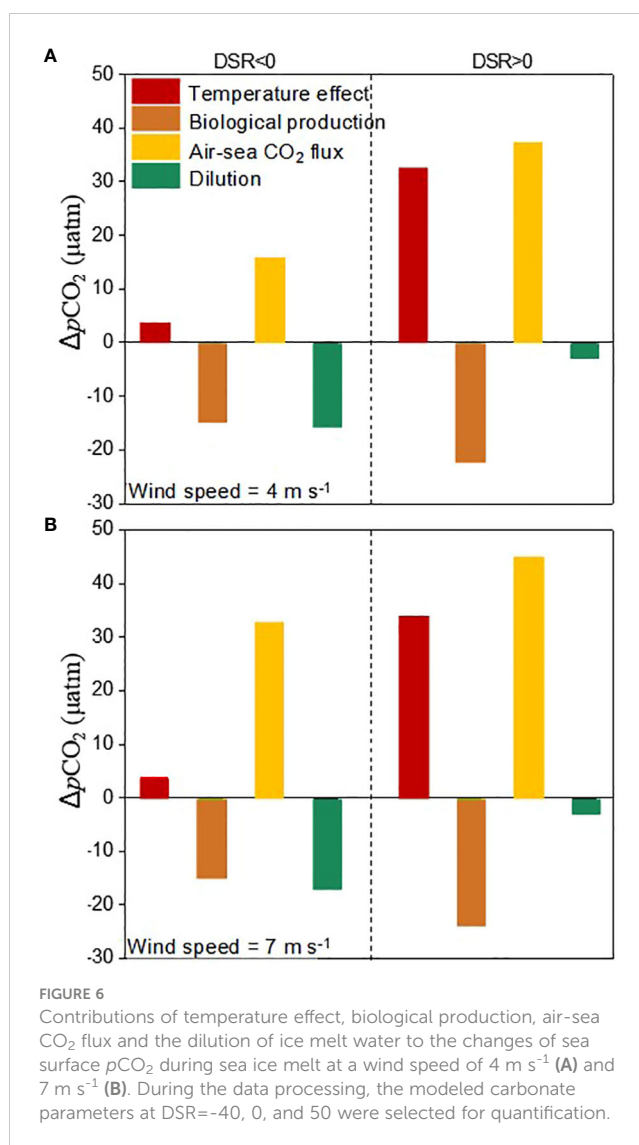


FIGURE 6 Contributions of temperature effect, biological production, air-sea CO_2 flux and the dilution of ice melt water to the changes of sea surface $p\text{CO}_2$ during sea ice melt at a wind speed of 4 m s^{-1} (A) and 7 m s^{-1} (B). During the data processing, the modeled carbonate parameters at $\text{DSR}=-40, 0$, and 50 were selected for quantification.

exchange result in a prevailing increase in sea surface $p\text{CO}_2$ during the post sea ice melt stage.

Compared to the average low wind speed of 4.0 m s^{-1} recorded during July and August in 2010, the enhanced CO_2 uptake at a high average wind speed of 7.0 m s^{-1} observed during July, August, and September in 2012 would further increase seawater $p\text{CO}_2$ by $17 \text{ } \mu\text{atm}$ during the active sea ice melt stage and by $8 \text{ } \mu\text{atm}$ during the post sea ice melt stage, while the contributions of temperature, biological production, and dilution from ice melt water remain constant (Figure 6B). During the active sea ice melt stage, although the presence of sea ice cover hinders air-sea CO_2 exchange at the sea surface, the increased wind speed from 4.0 m s^{-1} to 7.0 m s^{-1} and extremely low $p\text{CO}_2$ values (ranging from $320\text{--}330 \text{ } \mu\text{atm}$) tend to facilitate CO_2 dissolution into seawater and subsequently elevate the $p\text{CO}_2$ by $17 \text{ } \mu\text{atm}$. However, this wind-driven enhancement in CO_2 sinking is significantly attenuated with a $p\text{CO}_2$ increase of $8 \text{ } \mu\text{atm}$ during the post sea ice melt stage when $p\text{CO}_2$ values are considerably higher (ranging from $330\text{--}370 \text{ } \mu\text{atm}$).

4.2.3 Uncertainty analysis

In this study, the initial values utilized in model simulations were derived from a long-time field observation, which may differ from the observed values in a specific year. As previously discussed, we quantified the impact of varying wind speeds on $p\text{CO}_2$ dynamics, ranging from 53 to 77 μatm . Regarding the dilution effect, the mixing of ice melt water contributed to a $p\text{CO}_2$ variability of 18–43 μatm . For biological production, a low NCP of 1.88 $\text{mmol C m}^{-2} \text{d}^{-1}$ and a high NCP of 7 $\text{mmol C m}^{-2} \text{d}^{-1}$ was used in our $p\text{CO}_2$ simulation, indicating that biological processes could contribute to a $p\text{CO}_2$ variability of 37–137 μatm . Additionally, temperature effects were found to contribute significantly to a $p\text{CO}_2$ variability of 36–350 μatm . Therefore, careful selection of wind speeds, NCP values and the temperature range is crucial for achieving accurate model simulations.

5 Conclusion

This study presents the dynamics of sea surface $p\text{CO}_2$ during sea ice melt based on field measurements in the western Arctic Ocean. Compared to the $p\text{CO}_2$ reduction resulting from biological production and dilution effects, the contribution of air-sea CO_2 exchange is significantly lower. The combined effects of these factors have a significant impact on reducing $p\text{CO}_2$ during the active sea ice melt stage. In contrast, during the post sea ice melt stage, the increase in $p\text{CO}_2$ resulting from high temperatures and air-sea CO_2 exchange outweighs its decrease caused by biological production, dominating the prevailing increase in sea surface $p\text{CO}_2$. Compared to normal situations with a wind speed of 4.0 m s^{-1} , enhanced CO_2 uptake at a high wind speed of 7.0 m s^{-1} would further elevate seawater $p\text{CO}_2$ during both active and post sea ice melt stages. The increase in $p\text{CO}_2$ with high wind speed was more pronounced during active sea ice melt stage when seawater $p\text{CO}_2$ values were significantly lower. The present study reports, for the first time, the carbonate dynamics and controlling processes that govern $p\text{CO}_2$ dynamics during the active sea ice melt stage. It highlights the crucial role of wind speed in regulating the evolution of surface $p\text{CO}_2$ during sea ice melt.

In the Arctic Ocean, [Manizza et al. \(2019\)](#) also observed an exceptionally low SIC and relatively high levels of $p\text{CO}_2$ in the East Siberian Sea during 2012. Their findings indicated that the melt of sea ice under elevated seawater temperatures resulted in a substantial accumulation of freshwater on the sea surface. The presence of this low-density freshwater led to stratification within the water column, which hindered primary productivity of surface phytoplankton and impeded further reduction of $p\text{CO}_2$ through biotic processes, consequently leading to increased values of sea surface $p\text{CO}_2$. Our study argues that enhanced air-sea CO_2 uptake during periods characterized by

high wind speeds also contributed to the elevated levels of sea surface $p\text{CO}_2$ observed in 2012.

Data availability statement

The original contributions presented in the study are included in the article/Supplementary Material. Further inquiries can be directed to the corresponding author.

Author contributions

WY: Conceptualization, Methodology, Validation, Writing – original draft, Writing – review & editing. YZ: Conceptualization, Data curation, Methodology, Software, Validation, Writing – original draft, Writing – review & editing. YW: Conceptualization, Data curation, Methodology, Software, Supervision, Validation, Writing – original draft, Writing – review & editing. ZC: Data curation, Methodology, Software, Validation, Writing – original draft, Writing – review & editing. XG: Data curation, Software, Validation, Writing – original draft, Writing – review & editing. HL: Validation, Writing – original draft, Writing – review & editing. ZO: Conceptualization, Data curation, Methodology, Validation, Writing – original draft, Writing – review & editing. WC: Conceptualization, Methodology, Supervision, Validation, Writing – original draft, Writing – review & editing. LC: Conceptualization, Methodology, Writing – original draft, Writing – review & editing. DQ: Conceptualization, Formal analysis, Funding acquisition, Methodology, Project administration, Supervision, Validation, Writing – original draft, Writing – review & editing.

Funding

The author(s) declare financial support was received for the research, authorship, and/or publication of this article. This work was supported by the National Key Research and Development Program of China (2019YFE0114800), National Natural Science Foundation of China (42176230, 41941013), Fujian Provincial Science and Technology Plan (2022J06026), and Independent Research Projects of the Southern Marine Science and Engineering Guangdong Laboratory (Zhuhai) (SML2021SP306).

Acknowledgments

We thank the many contributors to the CHINARE dataset as well as the many research vessels and crews that contributed to the collection of data used in this study. We thank the Polar Research Institute of China and the Chinese National Arctic and Antarctic Data Center.

Conflict of interest

The authors declare that the research was conducted in the absence of any commercial or financial relationships that could be construed as a potential conflict of interest.

The handling editor, JC declared a past collaboration with the authors, DQ, YW, WC.

References

- Anderson, L., and Kaltin, S. (2016). Carbon fluxes in the Arctic Ocean-potential impact by climate change. *Polar Res.* 20 (2), 225–232. doi: 10.3402/Q26.polar.v20i2.6521
- Bates, N., Cai, J., and Mathis, J. (2011). The ocean carbon cycle in the Western Arctic Ocean: distributions and air-sea fluxes of carbon dioxide. *Oceanography* 24 (3), 186–201. doi: 10.5670/oceanog.2011.71
- Bates, N., and Mathis, J. (2009). The Arctic Ocean marine carbon cycle: evaluation of air-sea CO₂ exchanges, ocean acidification impacts and potential feedbacks. *Bioessences* 6 (11), 2433–2459. doi: 10.5194/bg-6-2433-2009
- Burgers, T., Miller, L., Thomas, H., Else, B., Gosselin, M., and Papakyriakou, T. (2017). Surface water pCO₂ variations and sea-air CO₂ fluxes during summer in the Eastern Canadian Arctic. *J. Geophys. Res.* 122, 9663–9678. doi: 10.1002/2017JC013250
- Cai, W., Chen, L., Chen, B., Gao, Z., Lee, S., Chen, J., et al. (2010). Decrease in the CO₂ uptake capacity in an ice-free Arctic Ocean Basin. *Science* 329, 556–559. doi: 10.1126/science.1189338
- Cross, J. N., Mathis, J. T., Frey, K. E., Cosca, C. E., Danielson, S. L., and Bates, N. R. (2014). Annual sea-air CO₂ fluxes in the Bering Sea: insights from new autumn and winter observations of a seasonally ice-covered continental shelf. *J. Geophys. Res. Oceans* 119, 6693–6708. doi: 10.1002/2013JC009579
- DeGrandpre, M., Evans, W., Timmermans, M., Krishfield, R., Williams, B., and Steele, M. (2020). Changes in the Arctic Ocean carbon cycle with diminishing ice cover. *Geophys. Res. Lett.* 47 (12), e2020GL088051. doi: 10.1029/2020GL088051
- DeGrandpre, M., Lai, C., Timmermans, M., Krishfield, R., Proshutinsky, A., and Torres, D. (2019). Inorganic Carbon and pCO₂ Variability during ice formation in the Beaufort Gyre of the Canada Basin. *J. Geophys. Res. Oceans* 124 (6), 4017–4028. doi: 10.1029/2019JC015109
- Dickson, A. (1990). Standard potential of the reaction: AgCl(s)+12H₂(g)=Ag(s)+HCl(aq), and the standard acidity constant of the ion HSO₄⁻ in synthetic sea water from 273.15 to 318.15 K. *J. Chem. Thermodyn* 22, 113–127. doi: 10.1016/0021-9614(90)90074-Z
- Dickson, A., and Millero, F. (1987). A comparison of the equilibrium constants for the dissociation of carbonic acid in seawater media. *Deep Sea Res. Part A Oceanographic Res. Papers* 34, 1733–1743. doi: 10.1016/0198-0149(87)90021-5
- Egleston, E. S., Sabine, C. L., and Morel, F. M. M. (2010). Revelle revisited: Buffer factors that quantify the response of ocean chemistry to changes in DIC and alkalinity. *Glob. Biogeochem. Cycles* 24, GB1002. doi: 10.1029/2008GB003407
- Fransson, A., Chierici, M., and Nojiri, Y. (2009). New insights into the spatial variability of the surface water carbon dioxide in varying sea ice conditions in the Arctic Ocean. *Cont Shelf Res.* 29, 1317–1328. doi: 10.1016/j.csr.2009.03.008
- Fransson, A., Chierici, M., Skjelvan, A., Olsen, P., Assmy, A., Peterson, G., et al. (2017). Effects of sea-ice and biogeochemical processes and storms on under-ice water fCO₂ during the winter-spring transition in the high Arctic Ocean: implications for sea-air CO₂ fluxes. *J. Geophys. Res. Oceans* 122, 5566–5587. doi: 10.1002/2016JC012478
- Friedlingstein, P., Jones, M., O' Sullivan, M., Andrew, R., Bakke, D., and Hauck, J. (2022). Global carbon budget 2021. *Earth Syst. Sci. Data* 14, 1917–2005. doi: 10.5194/essd-14-1917-2022
- García-Soto, C., Cheng, L., Caesar, L., Schmidt, S., Jewett, E., Cheripka, A., et al. (2021). An overview of ocean climate change indicators: sea surface temperature, ocean heat content, ocean pH, dissolved oxygen concentration, arctic sea ice extent, thickness and volume, sea level and strength of the AMOC (Atlantic meridional overturning circulation). *Front. Mar. Sci.* 21, 8–2021. doi: 10.3389/fmars.2021.642372
- Geilfus, N., Carnat, G., Papakyriakou, T., Tison, J., Else, B., Thomas, H., et al. (2012). Dynamics of pCO₂ and related air-ice CO₂ fluxes in the Arctic coastal zone (Amundsen Gulf, Beaufort Sea). *J. Geophys. Res.* 117, 1–15. doi: 10.1029/2011JC007118
- Harry, Y., Mcsween, J. R., Taylor, L. A., and Stolper, E. M. (1979). Carbon dioxide in the ocean surface: the homogeneous buffer factor. *Science* 204, 1203–1205. doi: 10.1126/science.204.4398.1203
- Islam, F., DeGrandpre, M., Beatty, C., Timmermans, M., Krishfield, R., Toole, J., et al. (2017). Sea surface pCO₂ and O₂ dynamics in the partially ice-covered Arctic Ocean. *J. Geophys. Res.* 122, 1425–1438. doi: 10.1002/2016JC012162
- Japan Meteorological Agency/Japan. (2013). *JRA-55: Japanese 55-year reanalysis, daily 3-hourly and 6-hourly data* (Boulder, CO: Research Data Archive, National Center for Atmospheric Research, Computational and Information Systems Laboratory).
- Jeong, S., Bloom, A., Schimel, D., Sweeney, C., Parazoo, N., Medvigy, D., et al. (2018). Accelerating rates of Arctic carbon cycling revealed by long-term atmospheric CO₂ measurements. *Sci. Adv.* 4 (7), ea01167. doi: 10.1126/sciadv.a01167
- Lindsay, R., and Schweiger, A. (2015). Arctic sea ice thickness loss determined using subsurface, aircraft, and satellite observations. *Cryosphere* 9 (1), 269–283. doi: 10.5194/tc-9-269-2015
- Manizza, M., Follows, M., Dutkiewicz, S., Menemenlis, D., Hill, C., and Key, R. (2013). Changes in the arctic ocean CO₂ sink, (1996-2007): a regional model analysis. *Global Biogeochem. Cycles* 27, 1108–1118. doi: 10.1002/2012GB004491
- Manizza, M., Menemenlis, D., Zhang, H., and Miller, C. (2019). Modeling the recent changes in the Arctic Ocean CO₂ sink, (2006-2013). *Global Biogeochem. Cycles* 33 (3), 420–438. doi: 10.1029/2018GB006070
- Mehrbach, C., Culbertson, C., Hawley, J., and Pytkowicz, R. (1973). Measurement of the apparent dissociation constants of carbonic acid in seawater at atmospheric pressure. *Limnol. Oceanogr.* 18, 897–907. doi: 10.4319/lo.1973.18.6.0897
- Mortenson, E., Steiner, N., Monahan, A., Hayashida, H., Sou, T., and Shao, A. (2020). Modeled impacts of sea ice exchange processes on Arctic Ocean carbon uptake and acidification, (1980-2015). *J. Geophys. Res. Oceans* 125, e2019JC015782. doi: 10.1029/2019JC015782
- Nomura, D., Eicken, H., Gradinger, R., and Shirasawa, K. (2010). Rapid physically driven inversion of the air-sea ice CO₂ flux in the seasonal landfast ice off Barrow, Alaska after onset of surface melt. *Cont Shelf Res.* 30, 1998–2004. doi: 10.1016/j.csr.2010.09.014
- Ouyang, Z., Li, Y., Qi, D., Zhong, W., Murata, A., Nishino, S., et al. (2022). The changing CO₂ sink in the Western Arctic Ocean from 1994 to 2019. *Global Biogeochem. Cycles* 36 (1), e2021GB007032. doi: 10.1029/2021GB007032
- Ouyang, Z., Qi, D., Chen, L., Takahashi, T., Zhong, W., DeGrandpre, M., et al. (2020). Sea-ice loss amplifies summertime decadal CO₂ increase in the western Arctic Ocean. *Nat. Clim. Chang* 10, 678–684. doi: 10.1038/s41558-020-0784-2
- Pierrot, D., Lewis, E., and Wallace, D. (2006). *MS Excel program developed for CO₂ system calculations*. Carbon Dioxide Information Analysis Center, Oak Ridge National Laboratory (Oak Ridge: U.S. Department of Energy). doi: 10.3334/cdiac/otg.co2sys_xls_cdiac105a
- Pipko, I., Pugach, S., Semiletov, I., Anderson, L., Shakhova, N., Gustafsson, Ö., et al. (2017). The spatial and inter-annual dynamics of the surface water carbonate system and air-sea CO₂ fluxes in the outer shelf and slope of the Eurasian Arctic Ocean. *Ocean Sci.* 13, 997–1016. doi: 10.5194/os-13-997-2017
- Polyakov, I., Rippeth, T., Fer, I., Alkire, M., Baumann, T., Carmack, E., et al. (2020). Weakening of cold halocline layer exposes sea ice to oceanic heat in the Eastern Arctic Ocean. *J. Clim.* 33 (18), 8107–8123. doi: 10.1175/JCLI-D-19-0976.1
- Qi, D., Chen, B., Chen, L., Lin, H., Gao, Z., Sun, H., et al. (2020). Coastal acidification induced by biogeochemical processes driven by sea-ice melt in the western Arctic ocean. *Polar Sci.* 23, 100504. doi: 10.1016/j.polar.2020.100504
- Qi, D., Ouyang, Z., Chen, L., Wu, Y., Lei, R., Chen, B., et al. (2022b). Climate change drives rapid decadal acidification in the Arctic Ocean from 1994 to 2020. *Science* 377 (6614), 1544–1550. doi: 10.1126/science.abo0383
- Qi, D., Wu, Y., Chen, L., Cai, W., Ouyang, Z., Zhang, Y., et al. (2022a). Rapid acidification of the arctic Chukchi Sea waters driven by anthropogenic forcing and biological carbon recycling. *Geophys. Res. Lett.* 49, e2021GL097246. doi: 10.1029/2021GL097246
- Riedel, A., Michel, C., Gosselin, M., and Leblanc, B. (2008). Winter-spring dynamics in sea-ice carbon cycling in the coastal Arctic Ocean. *J. Mar. Syst.* 74, 918–932. doi: 10.1016/j.jmarsys.2008.01.003
- Schuster, U., McKinley, G., Bates, N., Chevallier, F., Doney, S., Fay, A., et al. (2013). An assessment of the Atlantic and Arctic sea-air CO₂ fluxes 1990-2009. *Bioessences* 10, 607–627. doi: 10.5194/bg-10-607-2013
- Screen, J., and Simmonds, I. (2010). The central role of diminishing sea ice in recent Arctic temperature amplification. *Nature* 464 (7293), 1334–1337. doi: 10.1038/nature09051
- Semiletov, I., Makshtas, A., and Akasofu, S. (2004). Atmospheric CO₂ balance: The role of Arctic sea ice. *Geophys. Res. Lett.* 31, L05121. doi: 10.1029/2003GL019796

Publisher's note

All claims expressed in this article are solely those of the authors and do not necessarily represent those of their affiliated organizations, or those of the publisher, the editors and the reviewers. Any product that may be evaluated in this article, or claim that may be made by its manufacturer, is not guaranteed or endorsed by the publisher.

- Shepherd, A., Ivins, E., Barletta, V., Bentley, M., Bettadpur, S., Briggs, K., et al. (2012). A reconciled estimate of ice-sheet mass balance. *Science* 338 (6111), 1183–1189. doi: 10.1126/science.1228102
- Sun, H., Gao, Z., Peng, L., Xiu, P., and Chen, L. (2017). Evaluation of the net CO₂ uptake in the Canada Basin in the summer of 2008. *Hai Yang Xue Bao*. 36, 1–7. doi: 10.1007/s13131-017-1028-9
- Tu, Z., Le, C., Bai, Y., Jiang, Z., Wu, Y., Ouyang, Z., et al. (2021). Increase in CO₂ uptake capacity in the Arctic Chukchi Sea during summer revealed by satellite-based estimation. *Geophys. Res. Lett.* 48, e2021GL093844. doi: 10.1029/2021GL093844
- Uppstrom, L. (1967). "Analysis of boron in seawater by a modified curcumin method," in *Marine chemistry, vol. 1 (Analytical methods)*, 2nd ed, vol. 1972. Ed. D. F. Martin (New York: Marcei. Dekker. Inc), 389.
- Wanninkhof, R. (2014). Relationship between wind speed and gas exchange over the ocean revisited. *Limnol Oceanogr. Methods* 12, 351–362. doi: 10.4319/lom.2014.12.351
- Wanninkhof, R., Pierrot, D., Sullivan, K., Mears, P., and Barbero, L. (2022). Comparison of discrete and underway CO₂ measurements: inferences on the temperature dependence of the fugacity of CO₂ in seawater. *Mari Chem.* 247, 104178. doi: 10.1016/j.marchem.2022.104178
- Weiss, R. (1974). Carbon dioxide in water and seawater: the solubility of a nonideal gas. *Mar. Chem.* 2, 203–215. doi: 10.1016/0304-4203(74)90015-2
- Xu, A., Jin, M., Wu, Y., and Qi, D. (2023). Response of nutrients and primary production to high wind and upwelling favorable wind in the Arctic Ocean: A modeling perspective. *Front. Mar. Sci.* 10, 1065006. doi: 10.3389/fmars.2023.1065006
- Yang, W., Wu, Y., Cai, W., Ouyang, Z., Zhuang, Y., Chen, L., et al. (2023). Rapid changes in the surface carbonate system under complex mixing schemes across the Bering Sea: a comparative study of a forward voyage in July and a return voyage in September 2018. *Front. Mar. Sci.* 10, 1107646. doi: 10.3389/fmars.2023.1107646
- Yasunaka, S., Murata, A., Watanabe, E., Chierici, M., Fransson, A., Heuven, S., et al. (2016). Mapping of the air-sea CO₂ flux in the Arctic Ocean and its adjacent seas: Basin-wide distribution and seasonal to interannual variability. *Polar Res.* 10, 323–334. doi: 10.1016/j.polar.2016.03.006
- Yasunaka, S., Siswanto, E., Olsen, A., Hoppema, M., Watanabe, E., Fransson, A., et al. (2018). Arctic Ocean CO₂ uptake: an improved multiyear estimate of the air-sea CO₂ flux incorporating chlorophyll a concentrations. *Biogeosciences* 15, 1643–1661. doi: 10.5194/bg-15-1643-2018
- Zheng, Z., Luo, X., Wei, H., Zhao, W., and Qi, D. (2021). Analysis of the seasonal and interannual variations of air-sea CO₂ flux in the Chukchi Sea using a coupled ocean-sea ice-biogeochemical model. *J. Geophys. Res. Oceans* 126, e2021JC017550. doi: 10.1029/2021JC017550